Reduced ferroelectric coercivity in multiferroic $Bi_{0.825}Nd_{0.175}FeO_3$ thin film

G. L. Yuan, Siu Wing Or,[a] and Helen Lai Wa Chan
Department of Applied Physics, The Hong Kong Polytechnic University, Hung Hom, Kowloon, Hong Kong

Z. G. Liu
Laboratory of Solid State Microstructures, Nanjing University, Nanjing 210093, People's Republic of China

(Received 1 September 2006; accepted 3 November 2006; published online 17 January 2007)

$Bi_{0.825}Nd_{0.175}FeO_3$ (BNFO) thin film is grown on $Pt/TiO_2/SiO_2/Si$ substrate by pulsed laser deposition, and its multiferroic properties are compared with those of $BiFeO_3$ (BFO) thin film. With limited Fe^{2+} ions and its twinborn oxygen vacancies, both samples show low dielectric losses of <0.026 at 100 Hz and high maximum ferroelectric polarizations of $\sim 34\ \mu C/cm^2$. The ferroelectric coercive field of BNFO is reduced by $\sim 40\%$, reaching a low value of 235 kV/cm, compared to that of BFO due to the increased ratio of 180° and curved ferroelectric domains to total ferroelectric domains and better nucleation of the ferroelectric domains at the BNFO/Pt interface. The Raman scattering spectra confirm that the ferroelectric polarizations of both samples originate in the stereochemical activity of the Bi lone electron pair. Weak ferromagnetism is observed in both samples as a result of the limited amount of Fe^{2+} ions and γ-Fe_2O_3 impurity. © *2007 American Institute of Physics*. [DOI: 10.1063/1.2423228]

I. INTRODUCTION

$BiFeO_3$ (BFO) ceramics and single crystal show space-commensurate ferroelectricity below the Curie temperature of 1103 K and space-incommensurate antiferromagnetism below the Néel temperature of 643 K. The form of its spin is not collinear; it is essentially a spin cycloid with a wavelength of ~62 nm instead.[1] As a result, its remnant magnetization (M_r) and potential magnetoelectric effect both vanish on a macroscopic scale, giving rise to a quadratic ferromagnetoelectric behavior rather than a linear ferromagnetoelectric behavior.[2,3] By introducing thin-film epitaxial constraints,[4] by applying sufficiently large magnetic fields of 20 T,[5] or by chemical substitutions,[6–8] it is possible to destroy the spin cycloid and hence to release the nonzero macroscopic M_r and potential magnetoelectric effect. It has been demonstrated that *A*-site substituted BFO multiferroics (i.e., $Bi_{1-x}A_xFeO_3$, where *A* represents a nonmagnetic ion such as La^{3+}, Nd^{3+}, Sm^{3+}, or Ba^{3+} ion) accompany their nonzero macroscopic M_r with destroyed spin cycloids.[6–10]

However, the following three issues, which have been puzzling the community in recent years, need to be solved in order to release and measure simultaneous effects of ferroelectricity, piezoelectricity, and weak ferromagnetism. First, serious leakage current is a usual problem in $Bi_{1-x}A_xFeO_3$ multiferroics due to the presence of Fe^{2+} ions, oxygen vacancies (V_O^{2+}), low-resistive impurity phase, porosity, chemical fluctuation, interfacial charged defects, and interfacial roughness.[9,11–15] Second, in contrast with the generally low coercive field ($E_c < 100$ kV/cm) in common ferroelectric thin films, the inherently large E_c (>300 kV/cm) in BFO thin film always imposes tremendous difficulties on achieving a full polarization state even in relatively high-resistive samples.[9–11] Third, the high-resistive $Bi_{1-x}A_xFeO_3$ only allows weak ferromagnetism (with very small M_r),[6–8] although improved M_r (>10 emu/cm^3) can be achieved in low-resistive and deoxygenated $Bi_{1-x}A_xFeO_3$ thin films through the increased contributions of Fe^{2+} ions and γ-Fe_2O_3 impurity.[3,13–15] In this paper, we aim to analyze the origins of the three issues in $Bi_{0.825}Nd_{0.175}FeO_3$ (BNFO) and BFO thin films by comparing their crystal structures, leakage current densities, ferroelectricity, Raman scattering spectra, and weak ferromagnetism.

II. EXPERIMENTAL DETAILS

BNFO and BFO thin films were grown on $Pt/TiO_2/Ti/SiO_2/Si$ substrates for 25 min using a pulsed laser deposition (PLD) technique and Bi-rich targets of $Bi_{0.825\times1.1}Nd_{0.175}FeO_3$ and $Bi_{1\times1.1}FeO_3$ prepared by a rapid liquid-phase sintering method.[6–8] During the deposition, the substrate temperature was maintained at 580 °C with oxygen pressure of 20 Pa. The crystal structure and phase formation of the thin films were examined by an x-ray diffractometer (Brucker D8 advance system). The surface and sectional morphologies of the films were studied using a scanning electron microscope (Jeol JSM-6335F). Pt top electrodes of diameter of 200 μm were deposited on the films using the PLD technique. The electroded films were then annealed using a rapid thermal annealing (RTA) at 550 °C in air for 6 min. The dc electric field dependence of leakage current density (*J*-*E*) of the annealed films was measured using an electroceramic analyzer (aixACCT TF Analyzer 2000) with a voltage step of 0.1 V and a delay time of 0.2 s. The relative dielectric constant (ε) and loss tangent ($\tan\delta$) of the films were evaluated from 100 Hz to 1 MHz using an impedance analyzer (Agilent 4294A) with an oscillating voltage of 0.5 V peak. The polarization hysteresis (*P*-*E*) loops were acquired using the electroceramic analyzer operating in a vir-

[a]Author to whom correspondence should be addressed; electronic mail: apswor@polyu.edu.hk

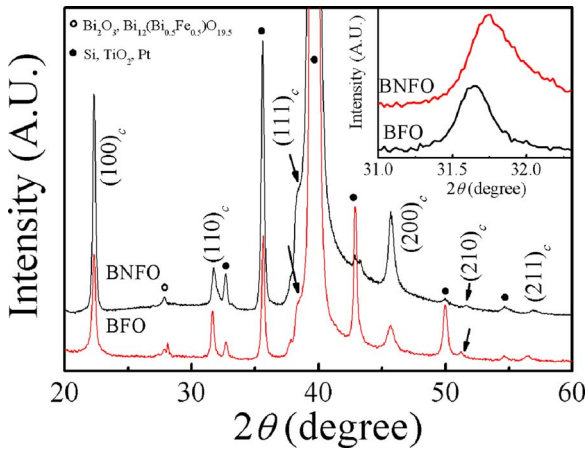

FIG. 1. (Color online) XRD patterns of BNFO and BFO thin films grown on $Pt/TiO_2/SiO_2/Si$ substrates, where the hollow circles indicate the diffraction peaks of Bi_2O_3 or $Bi_{12}(Bi_{0.5}Fe_{0.5})O_{19.5}$ impurities and the solid circles show the peaks of $Pt/TiO_2/SiO_2/Si$ substrate.

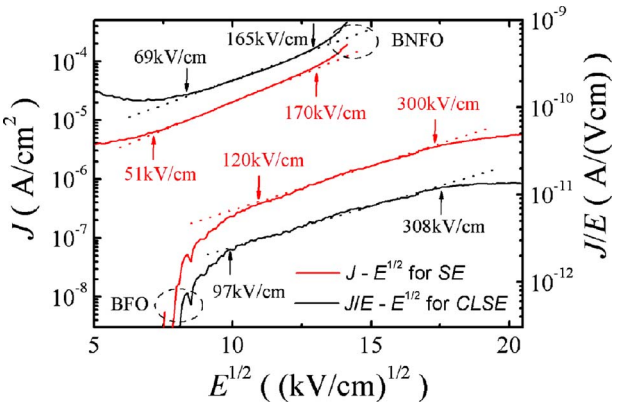

FIG. 2. (Color online) The characteristics of dc leakage current density (J), i.e., the dependence of J on $E^{1/2}$ for the Schottky emission (SE) conduction mechanism, and the dependence of J/E on $E^{1/2}$ for charge limited Schottky emission (CLSE) conduction mechanism, where the solid and dotted lines are obtained from the measurement and the fitting, respectively.

tual ground mode at 15 kHz. The magnetization hysteresis (M-H) loops were measured using a superconducting quantum interference device (Quantum Design XL7d) with an in-plane magnetic field of 12 kOe peak.

III. RESULTS AND DISCUSSION

The x-ray diffraction (XRD) patterns of BNFO and BFO thin films are shown in Fig. 1. Besides the peaks associated with the perovskite structure of BNFO and BFO thin films, an additional (small) peak at 2θ of $\sim 28°$ is detected in both samples. This peak may result from the presence of Bi_2O_3 and/or $Bi_{12}(Bi_{0.5}Fe_{0.5})O_{19.5}$ impurities since the deposition conditions used in the present study, including the Bi-rich targets, 580 °C substrate temperature, and 20 Pa oxygen pressure, are favorable for producing Bi-rich impurities and avoiding ferromagnetic γ-Fe_2O_3 impurity.[14,15] Like BFO ceramics and single crystal, the polycrystalline BFO thin film also exhibits a rhombohedrally distorted perovskite structure.[6,8] For our BNFO thin film, a shift of peak as manifested in the inset suggests a structural change from rhombohedral lattice to triclinic lattice owing to the A-site substitution effect of Nd^{3+} ion for Bi^{3+} ion,[6,8] while an increase in the full width at half maximum (FWHM) indicates a decrease in grain size. By observing their surface and sectional morphologies (not shown) using a scanning electron microscopy technique, it was found that our BNFO and BFO thin films have almost the same thickness of $\sim$600 nm in addition to grain sizes of 100–200 and 200–300 nm, respectively.

The dc leakage current density (J) is one of the most vital characteristics of ferroelectric thin films. The polarity-reversal of dc electric field (E) produces an asymmetric J-E curve as heating process of an interfacial layer near the bottom electrode is different from that near the top electrode. This asymmetric trait, together with a high work function of Pt metal, suggests that the most possible conduction mechanism for the high-E region should be governed by either the Schottky emission (SE) or the charge limited Schottky emission (CLSE).[16,17] Concerning CLSE, the mean free path of electrons injected from the cathode is less than the width of the Schottky barrier due to the low-density charged defects. Therefore, the other possibilities are excluded in our thin films even though the expression of Poole-Frenkel conduction mechanism is similar to that of CLSE. As the J-E characteristics of the SE and CLSE conduction mechanisms are characterized by the linear relationships of $\ln(J)$-$E^{1/2}$ and $\ln(J/E)$-$E^{1/2}$, respectively,[16,17] these two relationships are plotted in Fig. 2 along with the measured data. It is found that the $\ln(J)$-$E^{1/2}$ and $\ln(J/E)$-$E^{1/2}$ plots provide the most satisfactory descriptions to our BNFO and BFO thin films, respectively. This satisfaction suggests that the electrical conduction above the Ohmic region is mainly attributed to the SE conduction mechanism for BNFO thin film and the CLSE conduction mechanism for BFO thin film. In BFO thin film, a rather low J of $\sim 5.7\times10^{-6}$ A/cm^2 occurs at a superhigh E of 418 kV/cm. In BNFO thin film, J is almost two orders of magnitude higher than that of BFO thin film as a result of the increased charged defects and/or the increased roughness at the BNFO/Pt interface. Nevertheless, J of $\sim 1.9\times10^{-4}$ A/cm^2 at $E\sim 200$ kV/cm is still smaller than the data reported elsewhere,[18,19] reflecting the existence of relatively fewer Fe^{2+} ions and its twinborn V_O^{2+} vacancies in our BNFO thin film.

In Fig. 3, BNFO and BFO thin films have relative dielectric constant (ε) of $\sim$144 and $\sim$73, respectively, at 100 Hz. Their dielectric traits, such as low dielectric loss tangent ($\tan\delta$) of 0.026 at 100 Hz and the weak dependence of ε on frequency, indicate that dipoles with small effective masses (e.g., electrons and ferroelectric domain walls) mainly contribute to ε instead of charged defects with large effective masses (e.g., V_O^{2+} vacancy). Since large $\tan\delta$ at low frequencies and significant dependence of ε on frequency commonly reflect low electrical resistivity in BFO-based thin flims,[9,10,18] the observed dielectric traits should indicate the presence of high electrical resistivity in our BFNO and BFO thin films.

The polarization hysteresis (P-E) loops of BNFO and BFO thin films are shown in Fig. 4. It is clear that the P-E loops are well saturated. A left shift of P-E loops along the E

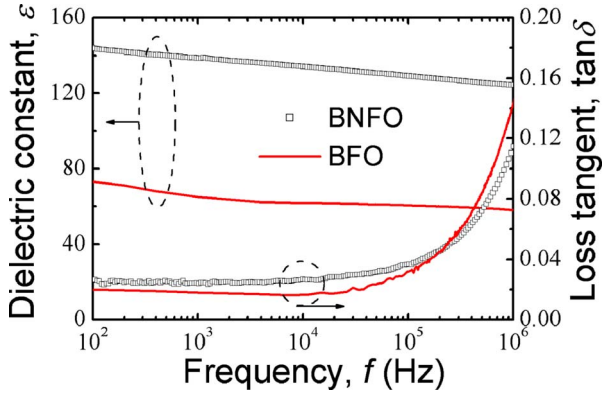

FIG. 3. (Color online) The relative dielectric constant (ε) and loss tangent ($\tan\delta$) of BNFO and BFO thin films in the frequency range of 100 Hz–1 MHz.

axis is due to the different heat processes for the top and bottom electrodes and the Schottky traits of SE and CLSE conduction mechanisms presented in our thin films. For BNFO thin film, the remnant polarization (P_r) of 27.3 μC/cm^2 and the maximum polarization (P_m) of 34.7 μC/cm^2 at the maximum electric field (E_m) of 665 kV/cm are obtained. BFO thin film has comparative P_r of 26.5 μC/cm^2 and P_m of 33.6 μC/cm^2 at E_m of 1000 kV/cm. However, it should be noted that the coercive field (E_c) of BNFO is ~235 kV/cm, which is ~40% smaller than the BFO's E_c of ~398 kV/cm. Besides the cause of lower E_m due to higher leakage current density in BNFO, the significant reduction in E_c should also originate from the following two facts.[19] First, the ratio of 180° and curved ferroelectric domains to total ferroelectric domains should be higher in BNFO thin film. For rhombohedral BFO thin film, there exists 71°, 109°, 180°, and curved ferroelectric domain switching.[20] As the switching of 71° and 109° ferroelectric domains is more difficult, 71° and 109° ferroelectric domains should play the main role in the high-E region. The switching of 180° and curved ferroelectric domains is relatively easy so that they should have the dominant effect in the low-E region. In fully oxygenated BFO thin film, the lower ratio of 180° and curved ferroelectric domains to total ferroelectric domains is one of the vital factors in producing super-high E_c. The crystal modulation as a result of the A-site

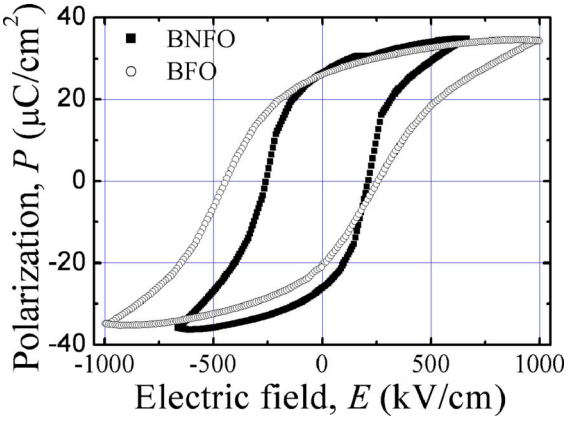

FIG. 4. (Color online) The polarization hysteresis (P-E) loops of BNFO and BFO thin films at 15 kHz.

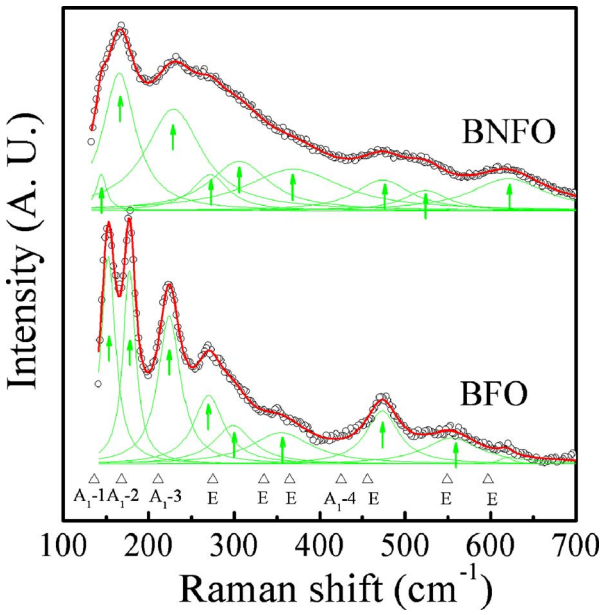

FIG. 5. (Color online) Measured Raman scattering spectra (open circles), together with their fitted spectra (thick solid line) and the decomposed active modes (thin solid lines and arrows), for BNFO and BFO thin films. The ten normal modes of the $(111)_c$-oriented $BiFeO_3$ epitaxial thin film with rhombohedral $R3c$ symmetry (open triangles and labels) are extracted from Ref. 22 for comparison with the samples.

substitution of Nd^{3+} ion (or La^{3+} ion in other reported works) for Bi^{3+} ion mainly enhances the ratio of 180° and curved ferroelectric domains to total ferroelectric domains in BFO-based thin films, leading to more difficulty in ferroelectric domain switching and hence a decrease in E_c.[19,21] It is interesting to note that the 71° and 109° ferroelectric domain switchings are generally unobservable in tetragonal ferroelectric thin films.[20] Second, an increase in charged defects and/or roughness at the BNFO/Pt interface not only increases the dc leakage current density upon field[12] but also favors the nucleation at the BNFO/Pt interface during the switching of ferroelectric domains, resulting in a reduction in E_c.

Figure 5 shows the measured Raman scattering spectra of BNFO and BFO thin films. By fitting the measured spectra and decomposing the fitted curves into individual Lorentzian components, the exact peaks, which represent the presence of Raman active modes, are obtained in both samples. It has been reported that the Raman active modes of BFO with rhombohedral $R3c$ symmetry can be summarized using the following irreducible representation: $\Gamma=4A_1+9E$.[22] For $(111)_c$-oriented $BiFeO_3$ epitaxial films with rhombohedral $R3c$ symmetry, there are ten normal modes, including A_1-1, A_1-2, and A_1-3 modes at 136, 168, and 211 cm^{-1}, respectively, with strong scattering intensity, A_1-4 mode at 425 cm^{-1} with quite weak scattering intensity, and six E modes at 275, 335, 365, 456, 549, and 597 cm^{-1} with medium scattering intensity.[22] These ten normal modes are also included in Fig. 5 for comparison with the decomposed active modes of our BNFO and BFO samples. On the basis of these normal modes, the first three peaks of our BNFO thin film at 144.3, 165.5, and 229.2 cm^{-1} are assigned as A_1 modes, while the later six peaks at 271.9, 306.0, 369.2, 473.7, 523.8, and 620.5 cm^{-1} are denoted as E modes. For

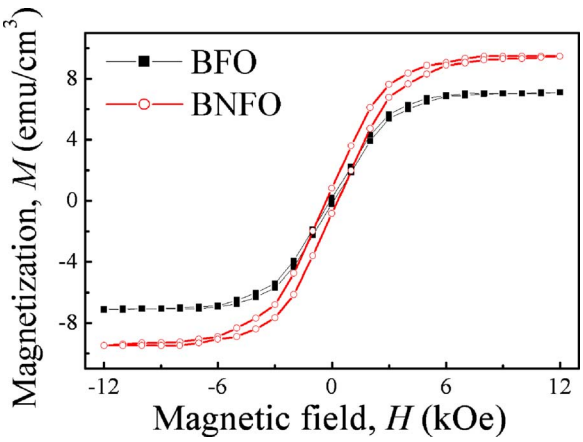

FIG. 6. (Color online) The magnetization hysteresis (*M-H*) loops of BNFO and BFO thin films.

BFO, similarly, the first three peaks at 152.6, 177.5, and 224.2 cm^{-1} are A_1 modes, and the subsequent six peaks at 270.0, 298.8, 354.9, 473.3, 554.3, and 618.3 cm^{-1} are *E* modes. Among these modes, the observed three A_1 modes as well as the *E* mode at ~270 cm^{-1} should be governed by the Bi–O covalent bonds which, in turn, are the origin of ferroelectric distortion.[23] The normal modes of BNFO, especially the A_1 mode at 144.3 cm^{-1} and the *E* mode at 271.9 cm^{-1}, exhibit much weaker scattering intensities than those of BFO. The phenomenon indicates less stable ferroelectric distortion of BNFO, which can be explained according to the change of Bi–O covalent bonds as a result of the decline in the stereochemical activity of the Bi lone electron pair.[2,23]

Figure 6 shows the magnetization hysteresis (*M-H*) loops of BNFO and BFO thin films. The two films exhibit weak ferromagnetism even though they have slight difference in saturation magnetization (M_s=7.2 emu/cm^3 for BFO and 9.5 emu/cm^3 for BNFO). Through analyzing our data and the results reported earlier,[3,11,13–15] the experimental results of BFO and $Bi_{1-x}A_xFeO_3$ thin films can generally be classified into two main types. For the first type, the fully oxygenated samples show high electrical resistivity so that the fully saturated *P-E* loops are achieved at E_m >500 kV/cm. However, only small M_s (e.g., <10 emu/cm^3) is permitted by the small canting angle of canted antiferromagnetism due to the absence of Fe^{2+} ion and γ-Fe_2O_3 impurity.[3,13–15] The slightly enhanced M_s and M_r (<10 emu/cm^3) are commonly realized by crystal modulation as a result of either substituting nonmagnetic Nd^{3+}, La^{3+}, Sm^{3+}, or Ba^{3+} ion or applying an external stress to epitaxial thin films.[3,10,13,14] Although crystal modulation can destroy spin cycloids and release macroscopic nonzero remnant magnetization, it cannot inhibit antiferromagnetic exchange interactions between occupied 3*d* orbits of Fe^{3+} ions or induce a prominent rise in canting angle.[3,13] For the second type, numerous Fe^{2+} ions in deoxygenated $Bi_{1-x}A_xFeO_3$ samples increase M_s to above 10 emu/cm^3 by destroying spin cycloids, increasing canting angle, and/or forming a net magnetic moment between Fe^{2+} and Fe^{3+} ions.[3,11,13] Since M_s is smaller than 9.5 emu/cm^3 in our BNFO and BFO samples, the magnetization contributions from Fe^{2+} ions and γ-Fe_2O_3 impurity are quite small.[3,11,13–15] The small increase in M_s in BNFO should mainly result from the collapse of spin cycloids. While the coexistence of large P_s and M_s has not been reported in high-resistive $Bi_{1-x}A_xFeO_3$ thin films, Fe^{2+} ions have shown to increase significantly in M_s at the expense of increasing V_O^{2-} vacancy and decreasing electrical resistivity.[2,3,15]

IV. CONCLUSION

We confirm the multiferroic properties of BNFO and compare them with these of BFO films. The ferroelectric coercive field of BNFO is smaller since 180° and curved ferroelectric domains increase and ferroelectric domains nucleate easier at the BNFO/Pt interface. The Raman spectra suggest that the ferroelectric distortion of BNFO is less stable than that of BFO due to the weakening of the stereochemical activity of the Bi lone electron pair and the change of the corresponding Bi–O bonds. As expected, weak ferromagnetism is achieved in fully oxygenated BNFO thin film.

ACKNOWLEDGMENTS

This work was supported by the Research Grants Council of the HKSAR Government under Grant Nos. PolyU 5255/03E and PolyU 5122/05E, the Center for Smart Materials of The Hong Kong Polytechnic University, and the National Natural Science Foundation of China under Grant No. 10374048.

[1] A. V. Zalesskii, A. A. Frolov, T. A. Khimich, and A. A. Bush, Phys. Solid State **45**, 141 (2003).
[2] M. Fiebig, J. Phys. D **38**, R123 (2005).
[3] W. Eerenstein, N. D. Mathur, and J. F. Scott, Nature (London) **442**, 759 (2006).
[4] F. M. Bai *et al.*, Appl. Phys. Lett. **86**, 032511 (2005).
[5] B. Ruette, S. Zvyagin, A. P. Pyatakov, A. Bush, J. F. Li, V. I. Belotelov, A. K. Zvezdin, and D. Viehland, Phys. Rev. B **69**, 064114 (2004).
[6] G. L. Yuan, S. W. Or, J. M. Liu, and Z. G. Liu, Appl. Phys. Lett. **89**, 052905 (2006).
[7] G. L. Yuan, K. Z. Baba-Kishi, J.-M. Liu, S. W. Or, Y. P. Wang, and Z. G. Liu, J. Am. Ceram. Soc. **89**, 3136 (2006).
[8] G. L. Yuan and S. W. Or, J. Appl. Phys. **100**, 024109 (2006).
[9] S. R. Das, P. Bhattacharya, R. N. P. Choudhary, and R. S. Katiyar, J. Appl. Phys. **99**, 066107 (2006).
[10] D. H. Wang, W. C. Goh, M. Ning, and C. K. Ong, Appl. Phys. Lett. **88**, 212907 (2006).
[11] J. Wang *et al.*, Science **307**, 1203b (2005).
[12] Y. H. Lee, J. M. Wu, Y. L. Chueh, and L. J. Chou, Appl. Phys. Lett. **87**, 172901 (2005).
[13] W. Eerenstein, F. D. Morrison, J. Dho, M. G. Blamire, J. F. Scott, and N. D. Mathur, Science **307**, 1203a (2005).
[14] H. Bea *et al.*, Appl. Phys. Lett. **87**, 072508 (2005).
[15] H. Bea, M. Bibes, S. Fusil, K. Bouzehouane, E. Jacquet, K. Rode, P. Bencok, and A. Barthelemy, Phys. Rev. B **74**, 020101 (2006).
[16] Y. P. Wang and T. Y. Tseng, J. Appl. Phys. **81**, 6762 (1997).
[17] F. D. Morrison, P. Zubko, D. J. Jung, J. F. Scott, P. Baxter, M. M. Saad, R. M. Bowman, and J. M. Gregg, Appl. Phys. Lett. **86**, 152903 (2005).
[18] K. Y. Yun, M. Noda, M. Okuyama, H. Saeki, H. Tabata, and K. Saito, J. Appl. Phys. **96**, 3399 (2004).
[19] H. Uchida, R. Ueno, H. Funakubo, and S. Koda, J. Appl. Phys. **100**, 014106 (2006).
[20] F. Zavaliche, P. Shafer, R. Ramesh, M. P. Cruz, R. R. Das, D. M. Kim, and C. B. Eom, Appl. Phys. Lett. **87**, 252902 (2005).
[21] Y. H. Lee, J. M. Wu, and C. H. Lai, Appl. Phys. Lett. **88**, 042903 (2006).
[22] M. K. Singh, H. M. Jang, S. Ryu, and M. H. Jo, Appl. Phys. Lett. **88**, 042907 (2006).
[23] M. K. Singh, S. Ryu, and H. M. Jang, Phys. Rev. B **72**, 132101 (2005).